Acta Oceanol. Sin., 2023, Vol. 42, No. 11, P. 59–68
https://doi.org/10.1007/s13131-023-2287-2
http://www.aosocean.com
E-mail: ocean2@hyxb.org.cn

Record of hydrothermal activity in the Yuhuang hydrothermal field and its implications for the Southwest Indian Ridge: evidence from sulfide chronology

Weifang Yang[1], Chunhui Tao[1,2]*, Shili Liao[1], Jin Liang[1], Wei Li[1], Teng Ding[3], Ágata Alveirinho Dias[4], Xuefeng Wang[5], Lisheng Wang[5]

[1] Key Laboratory of Submarine Geosciences, Second Institute of Oceanography, Ministry of Natural Resources, Hangzhou 310012, China

[2] School of Oceanography, Shanghai Jiaotong University, Shanghai 200030, China

[3] School of Marine Science and Engineering, Nanjing Normal University, Nanjing 210023, China

[4] Institute of Science and Environment, University of Saint Joseph, Macao 999078, China

[5] Key Laboratory of Cenozoic Geology and Environment, Institute of Geology and Geophysics, Chinese Academy of Sciences, Beijing 100029, China

Received 20 December 2022; accepted 16 March 2023

Abstract

The Yuhuang hydrothermal field (YHF) is located between the Indomed and Gallieni fracture zones near the top of the off-axis slope on the south rift wall of Segment 29 on the ultraslow Southwest Indian Ridge (SWIR). Previous studies have shown that sulfides in the YHF formed during different mineralization episodes and the YHF has the greatest potential for the formation of large-scale seafloor massive sulfide deposits. However, the sulfide chronology and hydrothermal activity of the YHF remain poorly constrained. In this study, mineralogical analyses and ^{230}Th/U dating were performed. Hydrothermal activity may start about (35.9 ± 2.3) ka from the southwest part of the YHF and may cease about (708 ± 81) a ago from the northeast part of the YHF. The 74 nonzero chronological data from hydrothermal sulfide samples provide the first quantitative characterization of the spatial and temporal history along the SWIR. Hydrothermal activity in the SWIR has been relatively active over the past 20 ka. In contrast, between 40 ka and 100 ka, hydrothermal activity was relatively infrequently and short in duration. The maximum activity occurred at 15–11 ka, 9–7 ka, 6–0.2 ka. There was a slight positive correlation between the maximal age and estimated surface area or estimated tonnage. The minimum mass accumulation rate of YHF is about 278 t/a, which is higher than most HFs related to ultramafic systems. The ultraslow spreading SWIR has the greatest potential to form large-scale seafloor massive sulfides (SMS) deposits. The results of this study provide new insights into the metallogenic mechanism of hydrothermal sulfides along ultraslow-spreading ridges.

Key words: Southwest Indian Ridge, seafloor massive sulfides, ^{230}Th/U dating, hydrothermal activity, mass accumulation

Citation: Yang Weifang, Tao Chunhui, Liao Shili, Liang Jin, Li Wei, Ding Teng, Dias Ágata Alveirinho, Wang Xuefeng, Wang Lisheng. 2023. Record of hydrothermal activity in the Yuhuang hydrothermal field and its implications for the Southwest Indian Ridge: evidence from sulfide chronology. Acta Oceanologica Sinica, 42(11): 59–68, doi: 10.1007/s13131-023-2287-2

1 Introduction

Polymetallic sulfides associated with submarine hydrothermal activity are rich in cooper (Cu), zinc (Zn), gold (Au), silver (Ag), cobalt (Co) and other elements, and represent a potential mineral resource. It is estimated that the total amount of sulfide in the submarine neovolcanic zones in the global oceans may reach 600 million tons and contain about 30 million tons of Cu and Zn (Hannington et al., 2011). In total, about 721 sites with seafloor hydrothermal venting at the seafloor have been discovered, including 666 active vent fields and 55 inactive vent fields. Among them, 404 sites are located along the mid-ocean ridges while 71 are at ultra-slow spreading midocean ridges (www.interridge.com).

The Southwest Indian Ridge (SWIR) is characterized by a heterogeneous magma supply along the ridge axis, which is composed alternately of magmatic-enriched and magmatic-barren Segments. The magmatic-barren segments often develop detachment faults and oceanic core complexes (Cannat et al., 1999; Sauter et al., 2001; Tao et al., 2012, 2020; Liu and Buck, 2018). Since 2007, many hydrothermal fields (HFs) have been discovered in the SWIR, including Longqi, Duanqiao, Yuhuang, Suye, Tianzuo and Tiancheng (Tao et al., 2012; Liao et al., 2018, 2022; Ding et al., 2021; Chen et al., 2018). Recent studies have shown that ultraslow spreading mid-ocean ridges also have the

Foundation item: The National Key R&D Program of China under contract No. 2022YFE0140200; the National Natural Science Foundation of China under contract Nos 42127807 and 42006074; the China Ocean Mineral Resources R&D Association Project under contract Nos DY135-S1-1-02 and DY135-S1-1-01;the Macao Science and Technology Development Fund under contract No. FDCT-002/2018/A1.

*Corresponding author, E-mail: taochunhuimail@163.com

potential to form large-scale sulfide deposits (Pedersen et al., 2010; Tao et al., 2012; Yu et al., 2021). For example, the ore-forming scale of Loki's Castle HF on the Arctic mid-ocean ridge is equivalent to the super-large sulfide deposits in the Trans-Atlantic Geotraverse (TAG) hydrothermal field in the Mid-Atlantic Ridge (Pedersen et al., 2010). The Yuhuang hydrothermal field (YHF) located on the south rift wall of segment 29 on the SWIR, is a detachment faulting hydrothermal system (Liao et al., 2018; Zhu et al., 2020a). Its estimated total resources are 10.6×10^6 t which may be considered as one of the largest seafloor massive sulfides (SMS) deposits (Yu et al., 2021). Sulfide geochemistry, sulfur and zinc isotope features of YHF have been studied and described different mineralization episodes that may form the different types of sulfides (Liao et al., 2018, 2019). However, the sulfide chronology and the hydrothermal activity of YHF remain poorly constrained compared with other HFs on the SWIR (e.g., Longqi, Duanqiao and Mt. Jourdanne) (Liang et al., 2018; Yang et al., 2017; Münch et al., 2001).

Chronology research can reveal multi-stage formation and superposition processes of ore bodies, as well as the formation and evolution history of sulfides, their growth and hydrothermal fluid activities more accurately (Lalou and Brichet,1982, 1987; Lalou et al., 1993, 1996; Kuznetsov et al., 2015; Wang et al., 2012; Jamieson et al., 2014). Limited chronological data on sulfides indicate that the maximum lifespan of a sulfide deposit is usually 100 000 a (Lalou et al., 1990, 1995; Cherkashov et al., 2010). In this study, mineralogical and chronological analyses were performed on four representative sulfides. We used the ^{230}Th/U dating method to constrain the sulfide formation history and the hydrothermal activity of YHF, and we coupled results of the estimated deposits tonnage to determine the accumulated rate of the sulfide deposits. We also established the relationship between the geological data and the surface area and resources. The results of this study provided new insights into the metallogenic mechanism of hydrothermal sulfides along ultra-slow spreading ridges.

2 Geological setting

As one of the major global plate boundaries, the SWIR separates the African and Antarctic plates, running from the Bouvet Triple Junction (55°S, 0°40′E) to the Rodrigues Triple Junction (25°30′S, 70°E) (Bach et al., 2002; Meyzen et al., 2003) (Fig. 1a). The SWIR has a full spreading rate of 14–18 mm/a, which varies slightly along the axial direction from N18°E to N0°E, which is a typical ultraslow spreading mid-ocean ridge (Dick et al., 2003). The average crust thickness of the SWIR is 4 km, which is much thinner than the average ocean crust thickness, and characterized by a lack of magmatic supply (Baker and German, 2004; Sauter and Cannat, 2010).

The YHF (37.94°S, 49.26°E) is located between the Indomed and Gallieni fracture zones near the top of the off-axis slope on the south rift wall of Segment 29 at a water depth of 1 400–1 900 m (Cannat et al., 1999; Sauter et al., 2001) (Fig. 1b). It is the shallowest mineralized area found in the SWIR. The YHF was first discovered in 2010 during the DY115-21 cruise R/V *Dayangyihao* (Han et al., 2010). Deep-tow camera, TV-grab sampling, and self-potential surveys have been conducted in 2014–2021 during the

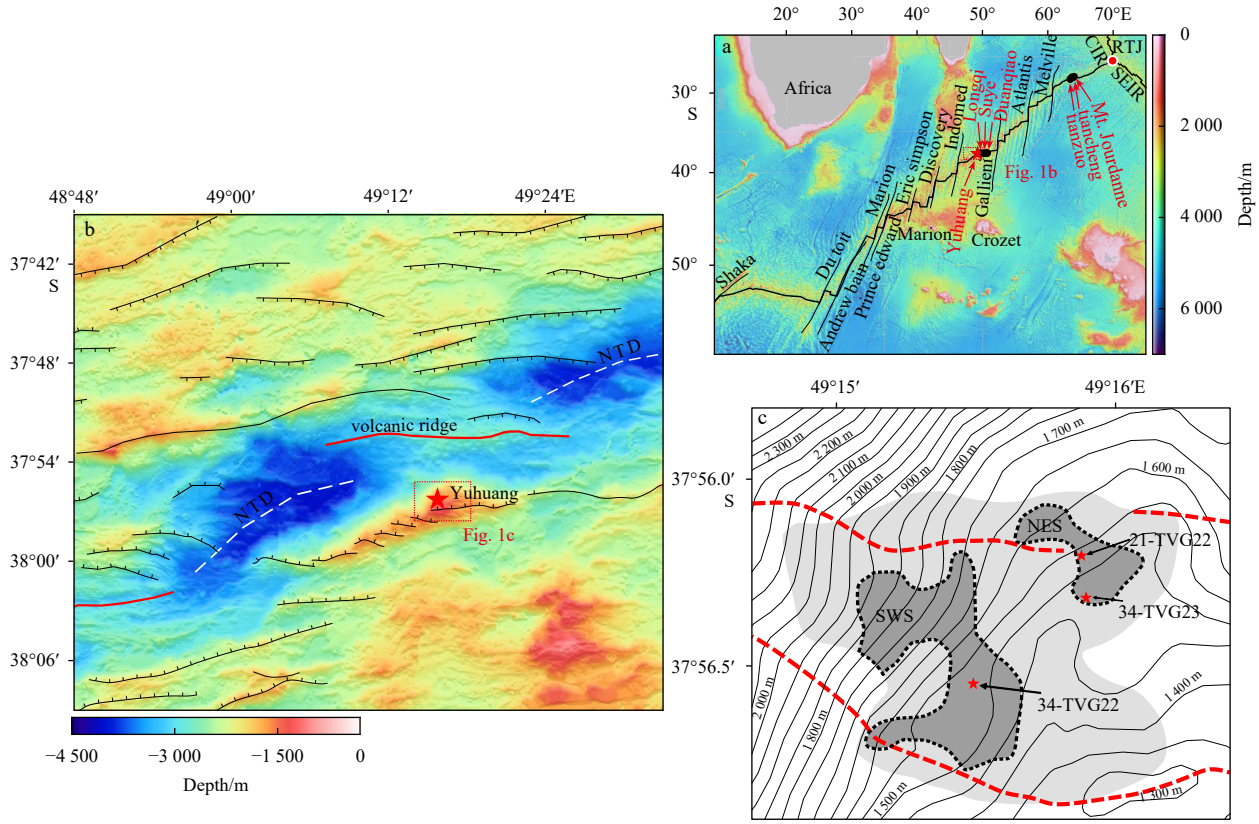

Fig. 1. Geological setting and topography of the study area. a. Geotectonic setting and topography of the Southwest Indian Ridge (SWIR) (modified from Yang et al., 2023). b. Shipboard bathymetric map of Yuhuang on the SWIR. c. The sampling stations in this study, all the others sampling stations can be seen in Yu et al. (2021). The red star in a represents the study area while the black dots represent the hydrothermal fields which have mentioned in this paper. White dotted lines in b and red dotted lines in c represent the non-transform discontinuity and inferred faults, respectively. Abbreviations: RTJ, Ridge Triple junction; CIR, Central Indian Ridge; SEIR, Southeast Indian Ridge.

DY34, DY39, DY40, DY43, DY52, DY58 and DY65 cruises. It is suggested the YH mineralization area can be divided into two sulfide accumulation areas including the northeast sulfide deposits (NES) and the southwest sulfide deposits (SWS). The NES area is relatively small compared to the SWS (Liao et al., 2018; Yu et al., 2021) (Fig. 1c). Samples of massive sulfides, sulfide rich chimneys, basalts, ultramafic rocks and hydrothermal sediments were obtained in this area by TV-grab sampling and shallow drilling by a robotic lander-type seafloor drilling rig (Yu et al., 2021).

3 Samples and analytical methods

3.1 *Sample collection and description*

The sulfide samples used in this study were collected by a TV grab during the DY115-21 and DY125-34 cruises of R/V *Dayangyihao*. Samples 34-TVG22-1 and 34-TVG22-2 were collected from the SWS, whereas samples 21-TVG22-1 and 34-TVG23-4 were recovered from the NES. All the sulfides were recovered at water depths between 1 440 m and 1 560 m (Fig. 1c). The pyritic massive sulfide sample (21-TVG22-3) has obvious three layers: pyrite-marcasite-sphalerite, sphalerite-pyrite and chalcopyrite-sphalerite (Fig. 2a). The silicified sulfide rich sample (34-TVG22-1) consists two parts: pyrite-sphalerite-marcasite-silicon and pyrite-marcasite-silicon (Fig. 2b). A small number of cellular fluid channels can also be seen inside the sample. The sphalerite-rich massive sulfide sample (34-TVG22-2) consists of a pyrite crust and a sphalerite core (Fig. 2c). Sample 34-TVG23-4 is a section of a silicified sulfide rich chimney (Fig. 2d).

3.2 *Analytical methods*

Mineral and textural examinations were described from polished thin sections using a reflected and transmitted light polarizing microscope (Zeiss AXIO Scope A1) at the Key Laboratory of Submarine Geosciences (Ministry of Natural Resources, Hangzhou, China).

Three whole-rock samples and thirteen micro-drilling samples were selected for ^{230}Th/U dating. The outer brown oxidation layers of the three whole-rock samples have been removed. And then the samples have been washed several times by de-ionized water in an ultrasonic bath. After drying, the samples were milled using a ball mill (mixer mill MM 200) for further analyses. The micro-drilling was carried out by a MICRODRILL SYSTEM at the State Key Laboratory of Ore Deposit Geochemistry, Institute of Geochemistry, Chinese Academy of Sciences. U and Th chemical separations and the mass spectrometry analyses were performed at the U-series chronology lab of Institute of Geology and Geophysics, (IGG) Chinese Academy of Sciences . A triple-spike (^{229}Th-^{233}U–^{236}U) isotope dilution method was employed to determine U/Th isotopic ratios and correct the instrumental fractionation. The chemical separation procedures were similar to those described in Yang et al. (2017) and Wang et al. (2021). Briefly, 20–50 mg samples were total digested with concentrated acid (HF/HNO_3/HCl). Then, the U and Th were purified and separated with 0.5 mL AG1-X8 resin. Finally, U and Th isotopes were analyzed using a Thermo Fisher NEPTUNE plus multi-collector inductively coupled plasma mass spectrometry (MC-ICP-MS) at IGG. The sample solution was introduced using a Polyfluoroalkoxy 50 μL/min nebulizer on an Aridus II desolvating nebulizer system. The instrumental parameters and procedures are described in Wang et al. (2021). ^{230}Th ages were calculated via equations presented in Edwards et al. (1987), Cheng et al. (2013), Yang et al. (2017) and Wang et al. (2021). A ^{230}Th age standard sample (GBW04412) was analyzed to verify the accuracy and precision of ^{230}Th/U dating. The precision of the method for ^{230}Th/U dating was better than 95%. All the results are within 2σ uncertainty, unless indicated. The chemical blanks for the entire process were 5–12 pg for ^{238}U, 0.5–1 fg for ^{230}Th and 3–5 fg for ^{232}Th, which were negligible for dating quaternary sulfide samples.

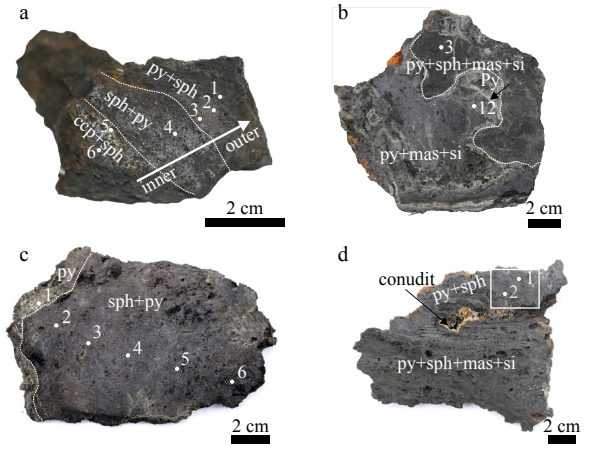

Fig. 2. Photographs of sulfides from the Yuhuang hydrothermal field (Modified from Liao et al., 2018). a–d represents sample 21-TVG22-3, 34-TVG22-1, 34-TVG22-2 and 34-TVG23-4, respectively. Mineral abbreviations: py, pyrite; ccp, chalcopyrite; mas, marcasite; sph, sphalerite; si, amorphous silica. The numbers indicate the microdrilling sample series for the dating analysis corresponding to Table 1.

4 Results

4.1 *Minerals*

The main mineral composition of pyritic massive sulfide sample (21-TVG22-3) consisted of pyrite (20%–30%), sphalerite (15%–20%) and chalcopyrite (8%–12%). Sphalerite coexists with the chalcopyrite (Fig. 3a). Pyrrhotite was rare in YHF sulfide samples (3%–5%), it is usually replaced by chalcopyrite (Fig. 3a). Pyrite was the most abundant sulfide phase in the silicified sulfide rich sample (34-TVG22-1). Based on the morphology, pyrite can be subdivided in three types: grained pyrite (Py1), coarse-grained pyrite (Py2), and colloform pyrite (Py3) (Fig. 3b). Pyrite generally coexisted with chalcopyrite and marcasite, which was often replaced by chalcopyrite (Figs 3c, d). Bornite often exhibited exsolution texture in chalcopyrite (Fig. 3d).

Sphalerite and pyrite were the main minerals in the sphalerite-rich massive sulfide sample (34-TVG22-2) while the chalcopyrite and bornite are less. The sphalerite exhibited two generations, early Sph1 and late Sph2 that is replaced by chalcopyrite and pyrite (Fig. 3e). The replacement of chalcopyrite with sphalerite was also observed (Figs 3e, f). Chalcopyrite has a bornite solid solution and growth edge (Figs 3e, f). The silicified sulfide rich chimney (34-TVG23-4) from the bottom part of a silicified chimney grew on basalt. Pyrite was often presented as a veined form in amorphous silicon and often replaced by sphalerite (Fig. 3g). Sphalerite had many generations and presented as banded aggregates (Fig. 3h). In addition, sphalerite was sometimes replaced by pyrite (Fig. 3i).

4.2 *U-Th isotope ratios and U-Th ages*

The U–Th isotope systematics of the samples are presented in Table 1. The U concentrations ranged from 35.1 × 10^{-9} to 39 847 × 10^{-9} for massive sulfide samples, with an average of 3 126.2 × 10^{-9}. The Th concentrations ranged from 276 × 10^{-12} to 2 723 × 10^{-12},

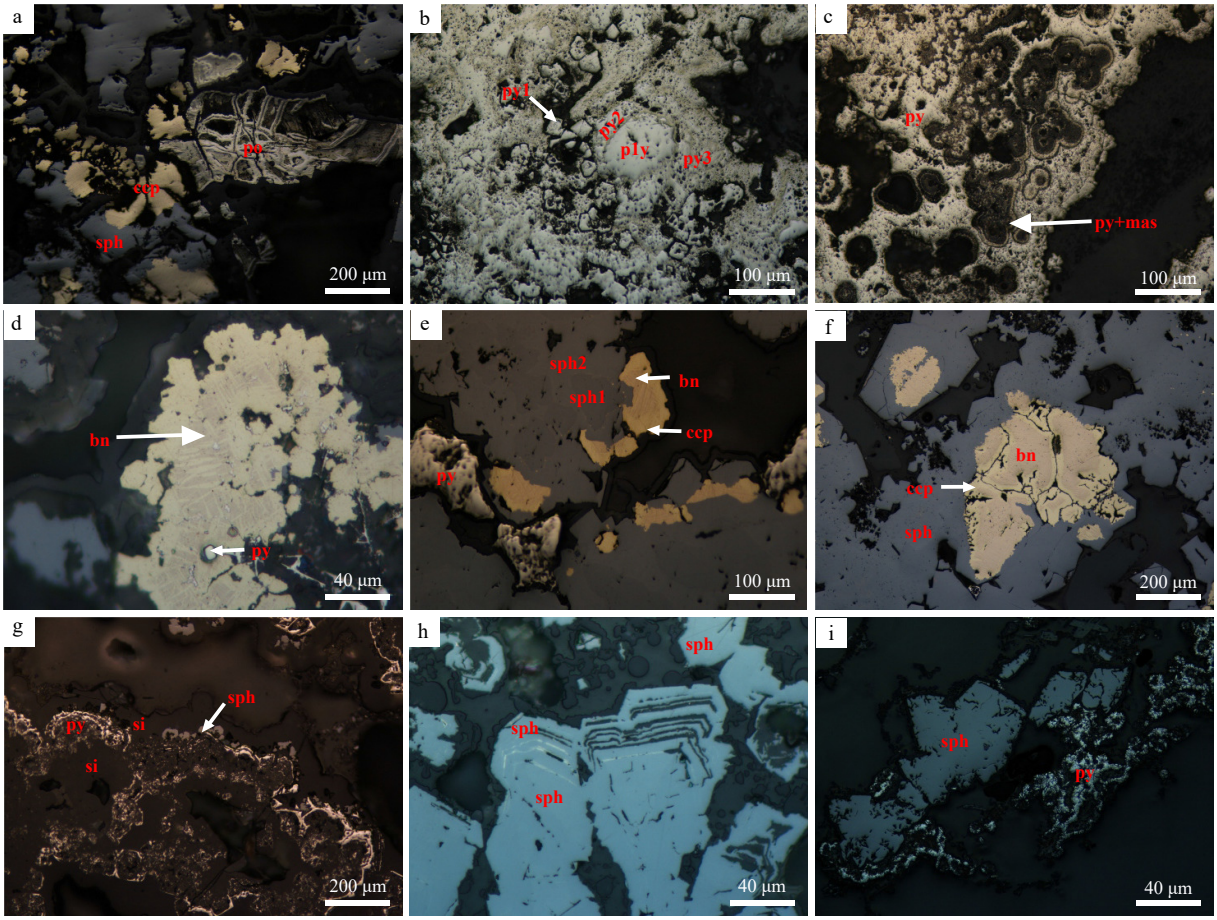

Fig. 3. Represent photomicrographs of sulfides from the Yuhuang hydrothermal field. a. Sphalerite coexisting with chalcopyrite and replacing pyrrhotite (21-TVG22-3). b. Typical varieties of pyrite: predominant fine-grained pyrite (py1), coarse-grained pyrite (py2), and colloform pyrite (py3) (34-TVG22-1). c. Colloform structure of pyrite and marcasite (34-TVG22-1). d. Pyrite replaced by chalcopyrite, and bornite replaced by chalcopyrite (34-TVG22-1). e. Sphalerite shows two generations (sph1 and sph2) that replaced by chalcopyrite, bornite replaced by chalcopyrite (34-TVG22-2). f. Chalcopyrite replaced by sphalerite, chalcopyrite has a bornite solid solution and growth edge (34-TVG22-2). g. Pyrite in the amorphous silica vein replaced by sphalerite (34-TVG23-4). h. Banded sphalerite (34-TVG23-4). i. Sphalerite replaced by pyrite (34-TVG23-4).

with an average of 685.3×10^{-12}. The U content was very low in subsamples 21-TVG22-3-4 (35.1×10^{-9}) and 34-TVG 22-2-4 (37×10^{-9}), but extremely high in subsample 21VII-TVG22-1. Also, most subsamples showed a significant positive correlation between U and Th (Fig. 4a). Notably, the $^{230}Th/^{232}Th$ ratios of most samples had a lower value, ranging from 19×10^{-6} to $3\,692 \times 10^{-6}$ which the $^{230}Th/^{232}Th$ ratio of 21VII-TVG22-1 can reach up to $198\,929.6 \times 10^{-6}$. Most of the measured $\delta^{234}U$ values range between 94 ± 24.4 and 150.5 ± 2.4, while the corrected $\delta^{234}U_{initial}$ range between 104 ± 27 and 156 ± 2 (Table 1). Most of the $\delta^{234}U_{initial}$ values are within the known range of seawater (149–155) and vent fluid (92–146) (Chen et al., 1986; Ludwig et al., 2011). The corrected ^{230}Th age of most subsamples from the massive sulfide 21-TVG22, 34-TVG23 and 34-TVG22 varied from (708 ± 81) a to (9 399 ± 374) a, (7 448 ± 59) a to (9 148 ± 59) a and (11 549 ± 59) a to (35 974 ± 2 312) a, respectively (Table 1). However, there was no systematic relationship between the ^{232}Th, ^{238}U, $\delta^{234}U_{initial}$ and the sample ages (Figs 4b–d).

5 Discussion

5.1 *Temporal evolution of hydrothermal activity in the YHF*

Complete geochronological data of sulfides from the YHF are given in Table 1. The oldest sulfide age was (35 974 ± 2 312) a and the sample originated from the southwest part, whereas the youngest sulfide (708 ± 81) a was from the northeast part of the YHF. Subsamples from the NES ranged from (708 ± 81) a to (9 418 ± 374) a while subsamples from the SWS ranged from (11 569 ± 59) a to (35 974 ± 2 312) a, demonstrating that NES sulfides are younger than SWS sulfides (Fig. 5a). Thus, it appears that mineralization in the YHF has shown spatial migration, progressing from the southwest towards the northeast. These results are consistent with sulfide Zn isotopes, which show significantly different values between the SWS and NES (Liao et al., 2019). This indicates that they are probably products of separate mineralization phases. The silicified sulfide-rich NES sample lacked characteristics for fluid venting and no active hydrothermal vents have been discovered in the SWS. All this evidence suggests that hydrothermal activity has likely ceased in these areas (Liao et al., 2019; Yu, 2022).

A preliminary data analysis suggests that hydrothermal activity may start about (35.9 ± 2.3) ka from the southwest part of the YHF and extended to the northeastern area by about (9.4 ± 0.4) ka. Hydrothermal activity likely ceased about (708 ± 81) a ago. The different temporal scale may represent the presence of hydrothermal activity during this period (Fig. 5b). However, because of

Table 1. U and Th and ^{230}Th ages for sulfide samples from Yuhuang hydrothermal field

Sample number	Longitude (°E)	Latitude (°S)	Depth/ m	^{238}U/ 10^{-9}	^{232}Th/ 10^{-12}	^{230}Th / ^{232}Th (atomic) / 10^{-6}	δ^{234}U* (measured)	^{230}Th / ^{238}U (activity)	^{230}Th age (uncorrected)/a	^{230}Th age (corrected)/a	δ^{234}Ui$_{nitial}$** (corrected)	^{230}Th age (corrected)/ (a BP)***
NES												
21-TVG22-1	49.265	37.939	1 443	39 847 ± 130	276 ± 10	198 929.6 ± 6 940.0	145 ± 2.1	0.083 6 ± 0.000 4	8 253 ± 42	8 253 ± 42	148 ± 2	8 233 ± 42
21-TVG22-2	49.265	37.939	1 443	1 126.5 ± 1.5	787 ± 16	1 846.4 ± 39.9	135.9 ± 2.4	0.078 2 ± 0.000 5	7 767 ± 56	7 749 ± 58	139 ± 2	7 729 ± 58
21-TVG22-3	49.265	37.939	1 443	139.6 ± 0.2	565 ± 12	386.5 ± 16.4	133.3 ± 5.1	0.094 9 ± 0.003 5	9 523 ± 367	9 419 ± 374	137 ± 5	9 399 ± 374
21-TVG22-3-1	49.265	37.939	1 443	124 ± 0.2	1 244 ± 27	50.3 ± 9.4	141.5 ± 5.2	0.030 6 ± 0.005 7	2 959 ± 560	2 703 ± 587	143 ± 5	2 682 ± 587
21-TVG22-3-2	49.265	37.939	1 443	791.4 ± 1.4	1 451 ± 30	73 ± 7.1	146.1 ± 3.3	0.008 1 ± 0.000 8	775 ± 74	729 ± 81	146 ± 3	708 ± 81
21-TVG22-3-3	49.265	37.939	1 443	70.1 ± 0.1	2 161 ± 44	19 ± 4.5	138.1 ± 8.6	0.035 5 ± 0.008 4	3 452 ± 828	2 662 ± 994	139 ± 9	2 641 ± 994
21-TVG22-3-4	49.265	37.939	1 443	35.1 ± 0.0	391 ± 9	48.7 ± 13.3	148.8 ± 7.2	0.032 8 ± 0.008 9	3 161 ± 872	2 879 ± 893	150 ± 7	2 858 ± 893
34-TVG23-4-1	49.265	37.937	1 557	1 419 ± 2.3	2 178 ± 45	991.8 ± 20.8	138.3 ± 2.1	0.092 3 ± 0.000 5	9 208 ± 52	9 169 ± 59	142 ± 2	9 148 ± 59
34-TVG23-4-2	49.265	37.937	1 557	1 107 ± 1.3	1 325 ± 28	1 046.3 ± 23.0	141.3 ± 1.7	0.075 9 ± 0.000 5	7 499 ± 55	7 469 ± 59	144 ± 2	7 448 ± 59
SWS												
34-TVG22-1-3	49.258	37.942	1 499	1 823.9 ± 3.0	2 723 ± 55	1 285.5 ± 26.2	150.5 ± 2.4	0.116 4 ± 0.000 4	11 606 ± 53	11 569 ± 59	156 ± 2	11 549 ± 59
34-TVG22-1-12	49.258	37.942	1 499	3 116.3 ± 5.2	2 081 ± 43	3 692.4 ± 77.4	136 ± 2.8	0.149 6 ± 0.000 7	15 353 ± 85	15 336 ± 86	142 ± 3	15 316 ± 86
34-TVG22-2-1	49.258	37.942	1 499	88.5 ± 0.2	464 ± 11	609.6 ± 26.6	132.1 ± 12.2	0.194 ± 0.007 2	20 418 ± 864	20 284 ± 868	140 ± 13	20 264 ± 868
34-TVG22-2-2	49.258	37.942	1 499	153.1 ± 0.2	1 066 ± 23	580.3 ± 22.6	135.2 ± 8.6	0.245 ± 0.007 9	26 380 ± 983	26 203 ± 989	146 ± 9	26 183 ± 989
34-TVG22-2-4	49.258	37.942	1 499	37 ± 0.1	419 ± 10	453.6 ± 24.5	94 ± 24.4	0.311 ± 0.015 1	36 292 ± 2 312	35 994 ± 2 312	104 ± 27	35 974 ± 2 312
34-TVG22-2-5	49.258	37.942	1 499	42.6 ± 0.2	447 ± 12	405.4 ± 34.5	126.7 ± 34.5	0.258 2 ± 0.020 9	28 241 ± 2 787	27 972 ± 2 783	137 ± 37	27 952 ± 2 783
34-TVG22-2-6	49.258	37.942	1 499	97.7 ± 0.1	240 ± 5	866.9 ± 27.0	148.7 ± 5.1	0.129 2 ± 0.002 8	12 974 ± 305	12 912 ± 308	154 ± 5	12 892 ± 308
Tianzuo HF												
20-S25-TVG21	63.533	27.85	3 630	2 745 ± 4	7 445 ± 149	2 670.2 ± 53.7	109.9 ± 1.6	0.439 2 ± 0.000 9	54 404 ± 177	54 334 ± 177	128 ± 2	54 314 ± 177
GBW04412	–	–	–	10 278 ± 14	5 821 ± 117	31 226.7 ± 631.2	852.4 ± 2.2	1.072 6 ± 0.002 1	87 046 ± 294	87 038 ± 294	1 090 ± 3	87 017 ± 294

Note: *$\delta^{234}U = [(^{234}U/^{238}U)_{activity} - 1] \times 1\,000$. ** $\delta^{234}U_{initial}$ was calculated based on ^{230}Th age (T), i.e., $\delta^{234}U_{initial} = \delta^{234}U_{measured} \times e_{\lambda 234} \times T$. Corrected ^{230}Th ages assume the initial $^{230}Th/^{232}Th$ atomic ratio of $(4.4 \pm 2.2) \times 10^{-6}$. Those are the values for a material at secular equilibrium, with the bulk earth $^{232}Th/^{238}U$ value of 3.8. The errors are arbitrarily assumed to be 50%. ***BP. stands for "before present" where the "present" is defined as the year 2000 A D. Sample 20-S25-TVG21 from Tianzuo hydrothermal field here is for later comparison and discussion.

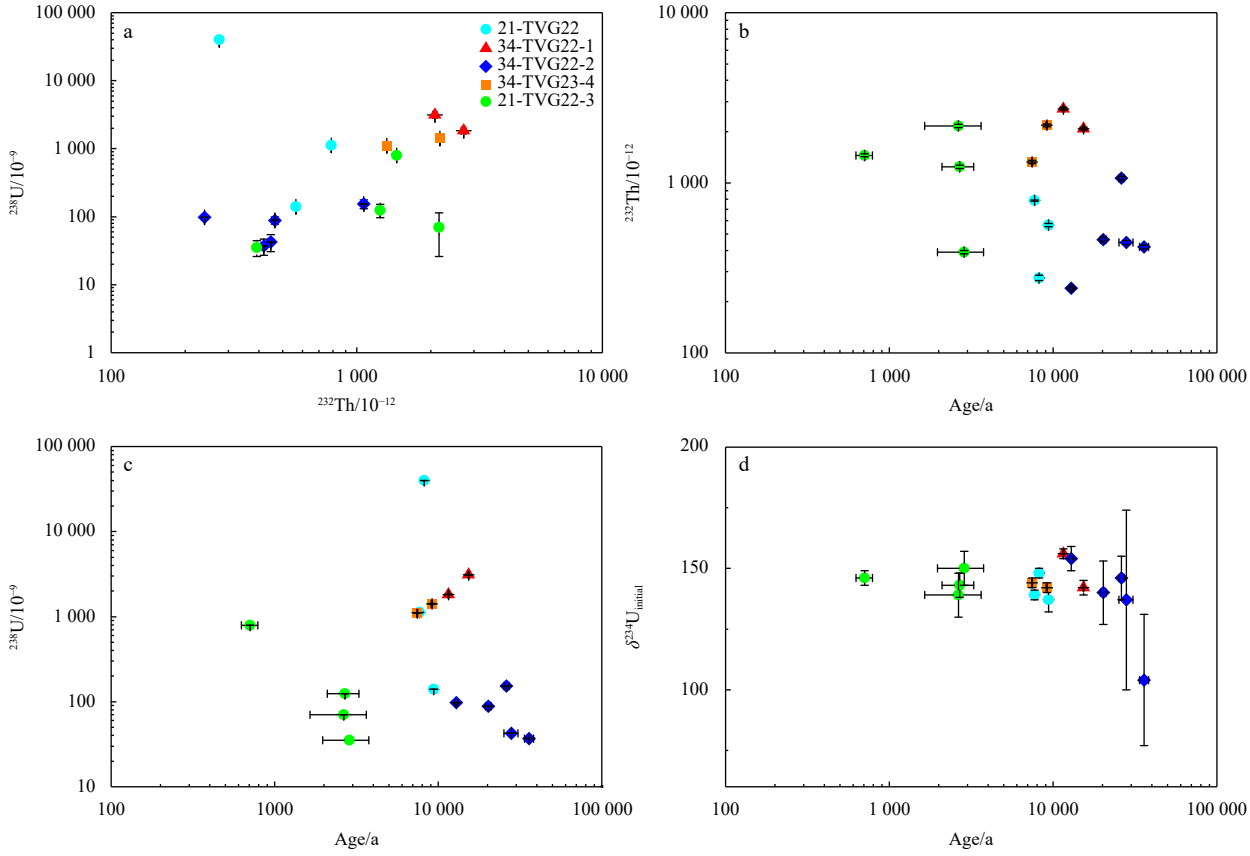

Fig. 4. The temporal variation of U–Th chemistry of sulfides from the Yuhuang hydrothermal field (YHF) the relationship between ^{232}Th and ^{238}U concentrations (a), age versus ^{232}Th (b), age versus ^{238}U (c) and age versus $\delta^{234}U_{initial}$ (d).

the small dataset, it is not possible to more precisely narrow down the active hydrothermal periods. Additionally, it is not possible to determine whether the venting was episodic or continuous from (35.9 ± 2.3) ka to (708 ± 81) a. The sulfur isotopes of the YHF sulfides are highly variable (–1.37‰ to 8.73‰), which may be related to the multi-stage hydrothermal activities (Liao et al., 2018). In the study area, both ultramafic rocks and basalts were exposed, indicating that detachment faults may be the main factor controlling hydrothermal activity in the YHF (Liao et al., 2018; Zhu et al., 2020b).

5.2 *Sulfide chronology along the SWIR*

From west to east along the SWIR, there are numerous HFs such as Yuhuang, Longqi, Duanqiao, Tianzuo, Mt. Jourdanne. In additional to the YHF and Tianzuo HF, we also collected fifty-six sulfide ages from Longqi, Duanqiao and Mt. Jourdanne HFs that has been reported so far (Yang et al., 2017; Liang et al., 2018; Münch et al., 2001). In total, these 74 nonzero chronological data from hydrothermal sulfide samples provide the first quantitative characterization of the spatial and temporal history along the SWIR (Fig. 6). Compared with Longqi, Duanqiao and Mt. Jourdanne, the sulfide formation in the YHF is relatively young. The only one dating result from the Tianzuo HF shows that the sulfide formation age is (54.3 ± 0.2) ka. Observations of significantly weathered sulfide and the presence of a thick sediment layer suggest that hydrothermal activity of Tianzuo HF ceased a long time ago (Chen et al., 2018). As a result of limited data from the Tianzuo HF, more samples are needed to expand our knowledge in this area.

The SWIR sulfide data indicate that hydrothermal events have been distributed unevenly through the time interval from 100 ka to 0.2 ka (Münch et al., 2001; Yang et al., 2017; Liang et al., 2018). Hydrothermal events in the SWIR demonstrate that over the past 20 ka, hydrothermal activity in the SWIR has been relatively active. In contrast, between 40 ka and 100 ka, hydrothermal activity was relatively infrequent and short in duration. The maximum activity occurred at 15–11 ka, 9–7 ka and 6–0.2 ka (Fig. 7). The ^{14}C dating of sediment cores in Longqi and Tianzuo HFs suggests that they have been affected by hydrothermal activity at ~8 ka and >45 ka, respectively (Huang, 2021). The accumulation and sediment redistribution of contourite drift have occurred throughout the last 40 ka of sediment deposition in the Southeast Indian Ridge (Dezileau et al., 2000).

YHF can be classified as the off-axis, detachment fault type. Longqi HF exhibits high-temperature hydrothermal vents and is associated with a major detachment fault system (Tao et al., 2012, 2020). The Duanqiao and Mt. Jourdanne HFs are typical local strong magma supply mineralization areas along the ridge axis (Tao et al., 2012; Yang et al., 2023; Münch et al., 2001; Nayak et al., 2014). Tianzuo HF is close to a non-transform discontinuity and far from the thermal activity controlled by the detachment fault system (Ding et al., 2021, Chen et al., 2018, Cao et al., 2021). Age data from all of the HFs indicate that hydrothermal activity lasted for thousands or even tens of thousands of years. The duration of this activity may provide favorable conditions for the formation of large sulfide deposits on the seafloor (Lalou et al., 1995; Jamieson et al., 2014; German et al., 2016).

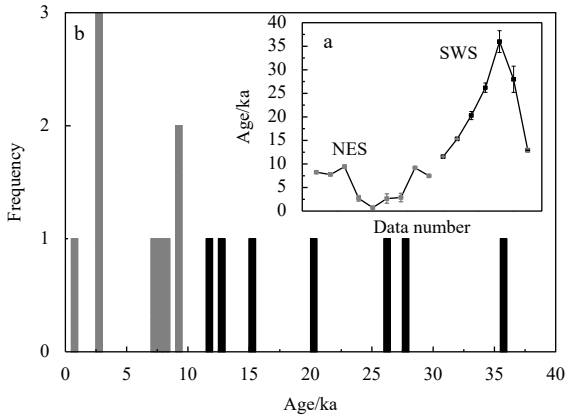

Fig. 5. Age distribution of hydrothermal sulfide samples from the Yuhuang hydrothermal field. a. Age error bar chart; b. distribution bar chart (gray: NES, black: southwest sulfide deposits).

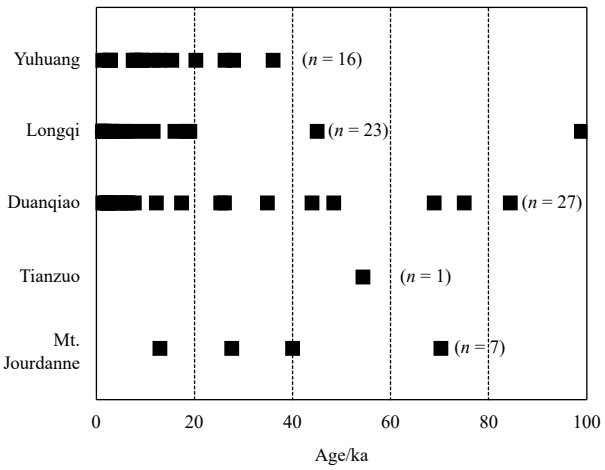

Fig. 6. Age distribution of hydrothermal sulfide samples from the Southwest Indian Ridge. Data base: Longqi (Liang et al., 2018); Duanqiao (Yang et al., 2017); Mt. Jourdanne (Münch et al., 2001).

5.3 *Correlation between the age, surface area and resource of hydrothermal sulfides along the mid-ocean ridge*

Previous studies have shown that time is crucial for the formation of large-scale ore deposits and the distribution scale of hydrothermal sulfide deposits along a mid-ocean ridge is closely related to the spreading rate of that ridge (Fouquet, 1997; Hannington et al., 2005; Cherkashov et al., 2017). The fast-spreading mid-ocean ridge is affected by frequent magmatic and tectonic processes and the duration of hydrothermal activity is short, so that the distribution area of sulfide formed by a magma chamber is often small (Fouquet, 1997; Hannington et al., 2011). In contrast, sulfide deposits formed along a slow-spreading mid-ocean ridge are large because of the long duration of hydrothermal activity (Petersen and Hein, 2013). We added the maximal ages and size of the ultraslow-spreading SWIR to available data of fast, intermediate, and slow-spreading ridges (Fig. 8). Compared with fast, intermediate, and slow-spreading ridges, the sulfide ages from the SWIR are relatively old. Hydrothermal fields, such as Yuhuang, Duanqiao and Tianzuo, are large and have good resource potential whereas the Mt. Jourdanne HF is small in scale and resource (Figs 8a, b). There was a slight positive correlation between the maximal age and estimated surface areas (n = 26, R^2 = 0.189) (Fig. 8a) as well as a weak positive correlation between the maximal age and estimated tonnage (n = 23, R^2 = 0.101) (Fig. 8b). Statistical analyses of maximal age and estimated surface area showed a relatively good positive correlation for HFs related to ultramafic-hosted systems (n = 13, R^2 = 0.393 3) while there was no correlation for basalt-hosted HFs (Fig. 8a). The relationships between estimated tonnage and the maximal age showed similar characteristics (Fig. 8b). Sulfide mineralization related to basalts typically form mounds, while sulfide mineralization with ultramafic rocks form relatively flat deposits (Fouquet et al., 2010). When using the same parameters, ultramafic-related deposits may provide a better approximation of the volume/resource available than basalt-related deposits (Cherkashov et al., 2017).

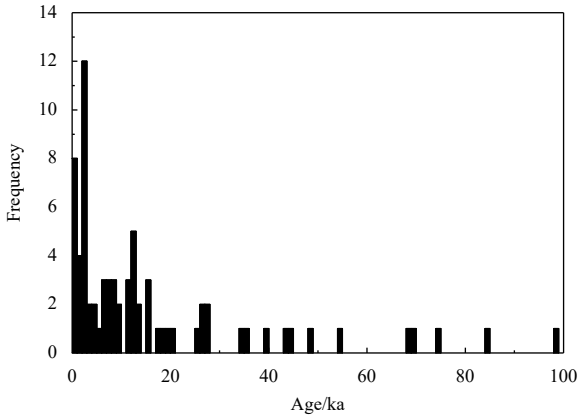

Fig. 7. Distribution bar chart of hydrothermal events during the last 100 ka in the Southwest Indian Ridge (SWIR).

Studies have shown that the estimated size of the YHF is 10 650 000–45 100 000 t, which is one of the largest SMS deposits worldwide (Yu et al., 2021). According to the maximal age and the minimum estimated size, the minimum mass accumulation rate of the YHF is about 278 t/a. This is higher than the accumulation rates related to most ultramafic HFs (Jamieson et al., 2014). Using the minimum mass accumulation rate, the sulfide resources of Duanqiao HF is estimated at 23 574 400 t. TAG mounds can contribute to a substantial accumulation of hydrothermal material (~29 Mt), which is comparable to other modern seafloor vent fields (Graber et al., 2020). These results further confirm that the ultraslow-spreading SWIR has a great potential to form large-scale SMS deposits. The YHF is located in the footwall of a detachment fault associated with basalts and ultramafic rocks which this is different from other ultraslow-spreading areas in its tectonic complexity (Liao et al., 2018, 2019). As a result of this complex geology, sulfide ore bodies in the YHF generally accumulated over long term in relatively small areas through multiple periods of hydrothermal activities. Serpentinization with deep ultramafic rocks provides a continuous heat source for the hydrothermal cycle, and accompanied by long-term hydrothermal activities, which makes the YHF more conducive to sulfide accumulation.

6 Conclusions

(1) The sulfides from the NES are younger than the SWS. Hydrothermal activity may start about (35.9 ± 2.3) ka from the southwest part of the YHF and may cease about (708 ± 81) ka ago from the northeast part of the YHF. The mineralization in the YHF shows spatial migration with hydrothermal mineralization first occurring in the southwest.

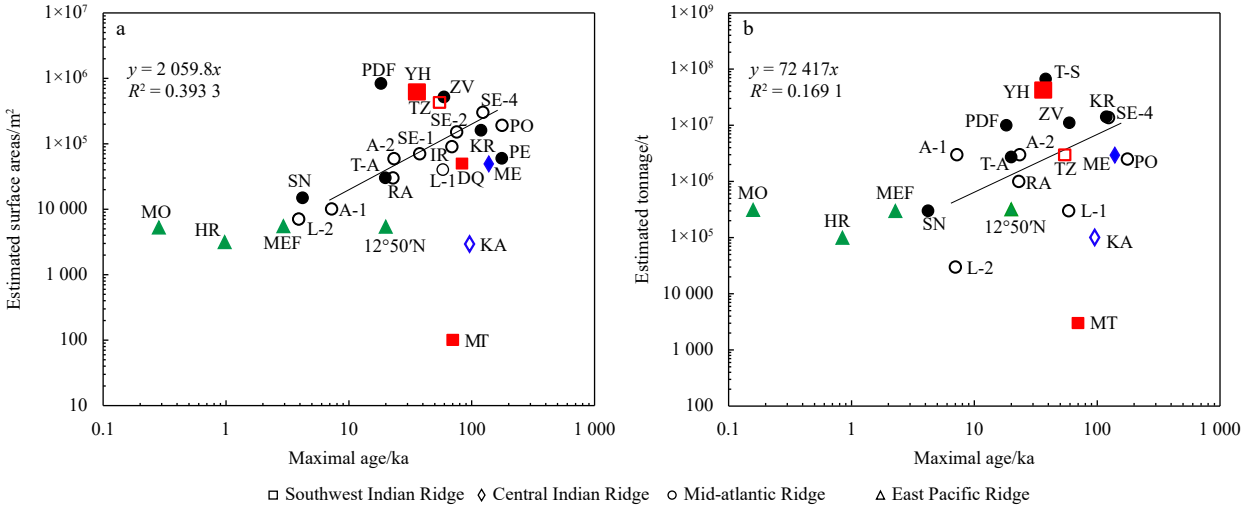

Fig. 8. Relationship between age and estimated surface areas (a) and estimated resources (b). The red, black, blue and green symbols represent the hydrothermal fields of ultraslow, slow, intermediate and fast spreading ridges, respectively. Filled symbols and empty symbols represent the basalts-hosted and ultramafic-hosted hydrothermal fields respectively. Abbreviations and data base: YH: Yuhuang (Yu et al., 2021; this study), DQ: Duanqiao(Yang et al., 2017, 2023), TZ: Tianzuo (Chen et al., 2018), MT: Mt. Jourdanne (Münch et al., 2001), KA: Kairei (Hannington et al., 2011; Wang et al., 2012), ME-Meso (Lalou et al., 1998; Hannington et al., 2011), SE-1: Semyenov-1, SE-2: Semyenov-2, SE-4: Semyenov-4, KR-Krasnow, ZV: Zenith-Victoria, IR: Irinovskoye, PE: Peterburgskoe, PDF: Puy des Folles, L-1: Logatchev-1, L-2: Logatchev-2, RA: Rainbow, A-1: Ashadze-1, A-2: Ashadze-2, SN: Snakepit, IR: Irinovskoye, PO: Pobeda (Hannington et al., 2011; Lalou et al., 1993, 1996; Cherkashov et al., 2010, 2017; Kuznetsov et al., 2011, 2015; Musatov and Cherkashov, 2020), T-A-TAG Active mound (Hannington et al.,1998; Lalou et al., 1995), T-S: TAG eSMS mounds (Murton et al., 2019; You and Bickle, 1998), LS: Lucky Stirke (Sánchez-Mora et al., 2022), MEF-Main Endeavour Field (Jamieson et al., 2013, 2014), HR: High Rise(Hannington et al., 2011; Jamieson et al., 2013), MO: Mothra(Hannington et al., 2011; Jamieson et al., 2013), 12°50′ (Lalou et al., 1985; Hannington et al., 2011). If the data is a range, take the maximal estimated surface areas or the maximal estimated resource in this figure.

(2) Hydrothermal activity in the SWIR has been relatively active over the past 20 ka, while during 40–100 ka, hydrothermal activity was relatively infrequent and short in duration. The maximum activity occurred at 15–11 ka, 9–7 ka and 6–0.2 ka.

(3) Hydrothermal fields, such as Yuhuang, Duanqiao and Tianzuo, are large and have good resource potential whereas the Mt. Jourdanne HF is small in scale and resource. Statistical analyses of maximal age and estimated surface area or tonnage show a relatively good positive correlation for HFs related to ultramafic-hosted systems while there was no correlation for basalt-hosted HFs.

(4) The minimum mass accumulation rate in the YHF was about 278 t/a, which is higher than most HFs related to ultramafic systems. Due to the complex geological structure of the YHF, sulfide ore bodies generally accumulate over longer periods of time in relatively small areas through multiple intervals of hydrothermal activity. Thus, the ultraslow spreading SWIR has a great potential to form large-scale SMS deposits.

Acknowledgements

We thank the captains, crew and the science parties who participated the DY115-21, DY125-34 cruises on R/V *Dayangyihao*. We are also grateful to three anonymous reviewers for their constructive comments and suggestions.

References

Bach W, Banerjee N R, Dick H J B, et al. 2002. Discovery of ancient and active hydrothermal systems along the ultra-slow spreading Southwest Indian Ridge 10–16°E. Geochemistry, Geophysics, Geosystems, 3(7): 1–14, doi: 10.1029/2001GC000279

Baker E T, German C R. 2004. On the global distribution of hydrothermal vent fields. In: German C R, Lin J, Parson L M, eds. Mid-Ocean Ridges: Hydrothermal Interactions Between the Lithosphere and Oceans. Washington: AGU, 245–266

Cannat M, Rommevaux-Jestin C, Sauter D, et al. 1999. Formation of the axial relief at the very slow spreading Southwest Indian Ridge (49° to 69°E). Journal of Geophysical Research: Solid Earth, 104(B10): 22825–22843, doi: 10.1029/1999jb900195

Cao Hong, Sun Zhilei, Jiang Zike, et al. 2021. Source origin and ore-controlling factors of hydrothermal sulfides from the Tianzuo hydrothermal field, Southwest Indian Ridge. Ore Geology Reviews, 134: 104168, doi: 10.1016/j.oregeorev.2021.104168

Chen Jie, Tao Chunhui, Liang Jin, et al. 2018. Newly discovered hydrothermal fields along the ultraslow-spreading Southwest Indian Ridge around 63°E. Acta Oceanologica Sinica, 37(11): 61–67, doi: 10.1007/s13131-018-1333-y

Chen J H, Wasserburg G J, von Damm K L, et al. 1986. The U–Th–Pb systematics in hot springs on the East Pacific Rise at 21°N and Guaymas Basin. Geochimica et Cosmochimica Acta, 50(11): 2467–2479, doi: 10.1016/0016-7037(86)90030-x

Cheng Hai, Edwards R L, Shen Chuanchou, et al. 2013. Improvements in ^{230}Th dating, ^{230}Th and ^{234}U half-life values, and U–Th isotopic measurements by multi-collector inductively coupled plasma mass spectrometry. Earth and Planetary Science Letters, 371–372: 82–91, doi: 10.1016/j.epsl.2013.04.006

Cherkashov G, Kuznetsov V, Kuksa K, et al. 2017. Sulfide geochronology along the Northern Equatorial Mid-Atlantic Ridge. Ore Geology Reviews, 87: 147–154, doi: 10.1016/j.oregeorev.2016.10.015

Cherkashov G, Poroshina I, Stepanova T, et al. 2010. Seafloor massive sulfides from the northern equatorial Mid-Atlantic Ridge: new discoveries and perspectives. Marine Georesources & Geotechnology, 28(3): 222–239, doi: 10.1080/1064119X.2010.483308

Dezileau L, Bareille G, Reyss J L, et al. 2000. Evidence for strong sediment redistribution by bottom currents along the Southeast In-

dian Ridge. Deep-Sea Research Part I, 47(10): 1899–1936, doi: 10.1016/S0967-0637(00)00008-X

Dick H J B, Lin Jian, Schouten H. 2003. An ultraslow-spreading class of ocean ridge. Nature, 426(6965): 405–412, doi: 10.1038/nature02128

Ding Teng, Tao Chunhui, Dias Á A, et al. 2021. Sulfur isotopic compositions of sulfides along the Southwest Indian Ridge: implications for mineralization in ultramafic rocks. Mineralium Deposita, 56(6): 991–1006, doi: 10.1007/s00126-020-01025-0

Edwards R L, Chen James H, Ku Teh-Lung, et al. 1987. Precise timing of the last interglacial period from mass spectrometric determination of thorium-230 in corals. Science, 236(4808): 1547–1553, doi: 10.1126/science.236.4808.1547

Fouquet Y. 1997. Where are the large hydrothermal sulphide deposits in the oceans?. Philosophical Transactions of the Royal Society A: Mathematical, Physical and Engineering Sciences, 355(1723): 427–441

Fouquet Y, Cambon P, Etoubleau J, et al. 2010. Geodiversity of hydrothermal processes along the Mid-Atlantic Ridge and ultramafic-hosted mineralization: A new type of oceanic Cu-Zn-Co-Au volcanogenic massive sulfide deposit. American Geophysical Union (AGU). 321–366, doi: 10.1029/2008GM000746

German C R, Petersen S, Hannington M D. 2016. Hydrothermal exploration of mid-ocean ridges: where might the largest sulfide deposits be forming?. Chemical Geology, 420: 114–126, doi: 10.1016/j.chemgeo.2015.11.006

Graber S, Petersen S, Yeo I, et al. 2020. Structural control, evolution, and accumulation rates of massive sulfides in the TAG hydrothermal field. Geochemistry, Geophysics, Geosystems, 21(9): e2020GC009185, doi: 10.1029/2020GC009185

Han Xiqiu, Wu Guanghai, Cui Ruyong, et al. 2010. Discovery of a hydrothermal sulfide deposit on the Southwest Indian Ridge at 49.2°E. In: Proceedings of the AGU Fall Meeting Abstracts, San Francisco, CA, USA, 13–17 December 2010. Washington, DC, USA: American Geophysical Union, p, OS21C–1531

Hannington M D, De Ronde C E J, Petersen S. 2005. Sea-floor tectonics and submarine hydrothermal systems. In: Hedenquist J W, Thompson J F H, Goldfarb R J, et al. , eds. One Hundredth Anniversary Volume. Littelton, Colorado, USA: Society of Economic Geologists, 111–141, doi: 10.5382/AV100.06

Hannington M D, Galley A G, Herzig P M, et al. 1998. Comparison of the TAG mound and stockwork complex with Cyprus-type massive sulfide deposits. In: Herzig P M, Humphris S E, Miller D J, et al. , eds. Proceedings of the Ocean Drilling Program, Scientific Results. San Antonio, Texas: Texas A & M University, 158: 389–415, doi: 10.2973/odp.proc.sr.158.217.1998

Hannington M, Jamieson J, Monecke T, et al. 2011. The abundance of seafloor massive sulfide deposits. Geology, 39(12): 1155–1158, doi: 10.1130/G32468.1

Huang Yongjin. 2021. Study on hydrothermal sedimentary records near the hydrothermal field of mafic and ultramafic rocks: a case study from Longqi and Tianzuo fields in the Southwest Indian Ridge (in Chinese)[dissertation]. Hangzhou: Second Institute of Oceanography, Ministry of Natural Resources

Jamieson J W, Clague D A, Hannington M D. 2014. Hydrothermal sulfide accumulation along the Endeavour Segment, Juan de Fuca Ridge. Earth and Planetary Science Letters, 395: 136–148, doi: 10.1016/j.epsl.2014.03.035

Jamieson J W, Hannington M D, Clague D A, et al. 2013. Sulfide geochronology along the Endeavour Segment of the Juan de Fuca Ridge. Geochemistry, Geophysics, Geosystems, 14(7): 2084–2099, doi: 10.1002/ggge.20133

Kuznetsov V, Maksimov F, Zheleznov A, et al. 2011. ^{230}Th/U chronology of ore formation within the semyenov hydrothermal district (13°31′N) at the Mid-Atlantic Ridge. Geochronometria, 38(1): 72–76, doi: 10.2478/s13386-011-0001-1

Kuznetsov V, Tabuns E, Kuksa K, et al. 2015. The oldest seafloor massive sulfide deposits at the Mid-Atlantic Ridge: ^{230}Th/U chronology and composition. Geochronometria, 42(1): 100–106, doi: 10.1515/geochr-2015-0009

Lalou C, Brichet E. 1982. Ages and implications of East Pacific Rise sulphide deposits 21°N. Nature, 300(5888): 169–171, doi: 10.1038/300169a0

Lalou C, Brichet E. 1987. On the isotopic chronology of submarine hydrothermal deposits. Chemical Geology: Isotope Geoscience Section, 65(3–4): 197–207, doi: 10.1016/0168-9622(87)90003-0

Lalou C, Brichet E, Hekinian R. 1985. Age dating of sulfide deposits from axial and off-axial structures on the East Pacific Rise near 12°50′N. Earth and Planetary Science Letters, 75(1): 59–71, doi: 10.1016/0012-821X(85)90050-0

Lalou C, Münch U, Halbach P, et al. 1998. Radiochronological investigation of hydrothermal deposits from the MESO zone, Central Indian Ridge. Marine Geology, 149(1–4): 243–254, doi: 10.1016/S0025-3227(98)00042-5

Lalou C, Reyss J L, Brichet E, et al. 1993. New age data for Mid-Atlantic Ridge hydrothermal sites: TAG and Snakepit chronology revisited. Journal of Geophysical Research: Solid Earth, 98(B6): 9705–9713, doi: 10.1029/92jb01898

Lalou C, Reyss J L, Brichet E, et al. 1995. Hydrothermal activity on a 10^5-year scale at a slow-spreading ridge, TAG hydrothermal field, Mid-Atlantic Ridge 26°N. Journal of Geophysical Research, 100(B9): 17855–17862, doi: 10.1029/95JB01858

Lalou C, Reyss J L, Brichet E, et al. 1996. Initial chronology of a recently discovered hydrothermal field at 14°45′N, Mid-Atlantic Ridge. Earth and Planetary Science Letters, 144(3–4): 483–490, doi: 10.1016/S0012-821X(96)00190-2

Lalou C, Thompson G, Arnold M, et al. 1990. Geochronology of TAG and Snakepit hydrothermal fields, Mid-Atlantic Ridge: witness to a long and complex hydrothermal history. Earth and Planetary Science Letters, 97(1–2): 113–128, doi: 10.1016/0012-821X(90)90103-5

Liang Jin, Tao Chunhui, Yang Weifang, et al. 2018. ^{230}Th/^{238}U dating of sulfide chimneys in the Longqi-1 hydrothermal field, Southwest Indian Ridge. Acta Geologica Sinica (English Edition), 92(S2): 77–78, doi: 10.1111/1755-6724.14202

Liao Shili, Tao Chunhui, Jamieson J W, et al. 2022. Oxidizing fluids associated with detachment hosted hydrothermal systems: example from the Suye hydrothermal field on the ultraslow-spreading Southwest Indian Ridge. Geochimica et Cosmochimica Acta, 328: 19–36, doi: 10.1016/j.gca.2022.04.025

Liao Shili, Tao Chunhui, Li Huaiming, et al. 2018. Bulk geochemistry, sulfur isotope characteristics of the Yuhuang-1 hydrothermal field on the ultraslow-spreading Southwest Indian Ridge. Ore Geology Review, 96: 13–27, doi: 10.1016/j.oregeorev.2018.04.007

Liao Shili, Tao Chunhui, Zhu Chuanwei, et al. 2019. Two episodes of sulfide mineralization at the Yuhuang-1 hydrothermal field on the Southwest Indian Ridge: Insight from Zn isotopes. Chemical Geology, 507: 54–63, doi: 10.1016/j.chemgeo.2018.12.037

Liu Zhonglan, Buck W R. 2018. Magmatic controls on axial relief and faulting at mid-ocean ridges. Earth and Planetary Science Letters, 491: 226–237, doi: 10.1016/j.epsl.2018.03.045

Ludwig K A, Shen Chuanzhou, Kelley D S, et al. 2011. U-Th systematics and ^{230}Th ages of carbonate chimneys at the lost city hydrothermal field. Geochimica et Cosmochimica Acta, 75(7): 1869–1888, doi: 10.1016/j.gca.2011.01.008

Meyzen C M, Toplis M J, Humler E, et al. 2003. A discontinuity in mantle composition beneath the Southwest Indian Ridge. Nature, 421(6924): 731–733, doi: 10.1038/nature01424

Münch U, Lalou C, Halbach P, et al. 2001. Relict hydrothermal events along the super-slow Southwest Indian spreading ridge near 63°56′E-mineralogy, chemistry and chronology of sulfide samples. Chemical Geology, 177(3–4): 341–349, doi: 10.1016/s0009-2541(00)00418-6

Murton B J, Lehrmann B, Dutrieux A M, et al. 2019. Geological fate of seafloor massive sulphides at the TAG hydrothermal field (Mid-Atlantic Ridge). Ore Geology Review, 107: 903–925, doi: 10.1016/j.oregeorev.2019.03.005

Musatov A E, Cherkashov G A. 2020. Influence of global glaciation on the origin of hydrothermal activity within the Mid-Atlantic Ridge. Oceanology, 60(3): 405–411, doi: 10.1134/S0001437020030066

Nayak B, Halbach P, Pracejus B, et al. 2014. Massive sulfides of Mount Jourdanne along the super-slow spreading Southwest Indian Ridge and their genesis. Ore Geology Reviews, 63: 115–128, doi: 10.1016/j.oregeorev.2014.05.004

Pedersen R B, Rapp H T, Thorseth I H, et al. 2010. Discovery of a black smoker vent field and vent fauna at the Arctic Mid-Ocean Ridge. Nature Communications, 1(1): 126, doi: 10.1038/NCOMMS1124

Petersen S, Hein J R. 2013. Deep Sea Minerals: Sea-Floor Massive Sulphides; A Physical, Biological, Environmental, and Technical Review. Secretariat of the Pacific Community, GRID-Arendal, Chapter1: 7–18.

Sánchez-Mora D, Jamieson J, Cannat M, et al. 2022. Age and rate of accumulation of metal-rich hydrothermal deposits on the seafloor: the lucky strike vent field, Mid-Atlantic Ridge. Journal of Geophysical Research: Solid Earth, 127(6): e2022JB024031, doi: 10.1029/2022JB024031

Sauter D, Cannat M. 2010. The ultraslow spreading Southwest Indian Ridge. In: Rona P A, Devey C W, Dyment J, et al., Eds. Diversity of Hydrothermal Systems on Slow Spreading Ocean Ridges. Washington: AGU, 153–173, doi: 10.1029/2008GM000843

Sauter D, Patriat P, Rommevaux-Jestin C, et al. 2001. The Southwest Indian Ridge between 49°15′ E and 57°E: focused accretion and magma redistribution. Earth and Planetary Science Letters, 192(3): 303–317, doi: 10.1016/s0012-821x(01)00455-1

Tao Chunhui, Lin Jian, Guo Shiqin, et al. 2012. First active hydrothermal vents on an ultraslow-spreading center: Southwest Indian Ridge. Geology, 40(1): 47–50, doi: 10.1130/G32389.1

Tao Chunhui, Seyfried W E Jr, Lowell R P, et al. 2020. Deep high-temperature hydrothermal circulation in a detachment faulting system on the ultra-slow spreading ridge. Nature Communication, 11(1): 1300, doi: 10.1038/s41467-020-15062-w

Wang Yejian, Han Xiqiu, Jin Xionglong, et al. 2012. Hydrothermal activity events at Kairei field, Central Indian Ridge 25°S. Resource Geology, 62(2): 208–214, doi: 10.1111/j.1751-3928.2012.00189.x

Wang Lisheng, Sun Zhilei, Cao Hong, et al. 2021. A new method for the U-Th dating of a carbonate chimney deposited during the Last Glaciation in the northern Okinawa Trough, East China Sea. Quaternary Geochronology, 66: 101199, doi: 10.1016/j.quageo.2021.101199

Yang Weifang, Liao Shili, Dias Á A, et al. 2023. Geochemistry, sulfur and lead isotopic composition of hydrothermal sulfide from the Duanqiao hydrothermal field on the Southwest Indian Ridge: implications for ore genesis. International Geology Review, 65(6): 883–899, doi: 10.1080/00206814.2022.2081937

Yang Weifang, Tao Chunhui, Li Huaiming, et al. 2017. $^{230}Th/^{238}U$ dating of hydrothermal sulfides from Duanqiao hydrothermal field, Southwest Indian Ridge. Marine Geophysical Research, 38(1–2): 71–83

You C F, Bickle M J. 1998. Evolution of an active sea-floor massive sulphide deposit. Nature, 394(6694): 668–671, doi: 10.1038/29279

Yu Junyu. 2022. Enrichment and migration of ore-forming elements in Yuhuang-1 hydrothermal field at ultraslow-spreading Southwest Indian Ridge (in Chinese)[dissertation]. Hangzhou: Zhejiang University

Yu Junyu, Tao Chunhui, Liao Shili, et al. 2021. Resource estimation of the sulfide-rich deposits of the Yuhuang-1 hydrothermal field on the ultraslow-spreading Southwest Indian Ridge. Ore Geology Reviews, 134: 104169, doi: 10.1016/j.oregeorev.2021.104169

Zhu Zhongmin, Tao Chunhui, Shen Jinsong, et al. 2020a. Self-potential tomography of a deep-sea polymetallic sulfide deposit on Southwest Indian Ridge. Journal of Geophysical Research:Solid Earth, 125(11): e2020JB019738, doi: 10.1029/2020JB019738

Zhu Chuanwei, Tao Chunhui, Yin Runsheng, et al. 2020b. Seawater versus mantle sources of mercury in sulfide-rich seafloor hydrothermal systems, Southwest Indian Ridge. Geochimica et Cosmochimica Acta, 281: 91–101, doi: 10.1016/j.gca.2020.05.008